Available online at www.sciencedirect.com
ScienceDirect
Journal of Bionic Engineering 14 (2017) 336–347

Motion Control in Saccade and Smooth Pursuit for Bionic Eye Based on Three-dimensional Coordinates

Qingbin Wang[1,2], Wei Zou[1,2], De Xu[1,2], Zheng Zhu[1,2]

1. *Research Center of Precision Sensing and Control*, *Institute of Automation*, *Chinese Academy of Sciences*, *Beijing* 100190, *China*
2. *University of Chinese Academy of Sciences*, *Beijing* 100190, *China*

Abstract

Saccade and smooth pursuit are two important functions of human eye. In order to enable bionic eye to imitate the two functions, a control method that implements saccade and smooth pursuit based on the three-dimensional coordinates of target is proposed. An optimal observation position is defined for bionic eye based on three-dimensional coordinates. A kind of motion planning method with high accuracy is developed. The motion parameters of stepper motor consisting of angle acceleration and turning time are computed according to the position deviation, the target's angular velocity and the stepper motor's current angular velocity in motion planning. The motors are controlled with the motion parameters moving to given position with desired angular velocity in schedule time. The experimental results show that the bionic eye can move to optimal observation positions in 0.6 s from initial location and the accuracy of 3D coordinates is improved. In addition, the bionic eye can track a target within the error of less than 20 pixels based on three-dimensional coordinates. It is verified that saccade and smooth pursuit of bionic eye based on three-dimensional coordinates are feasible.

Keywords: bionic eye, saccade, smooth pursuit, motion planning, observation position

Copyright © 2017, Jilin University. Published by Elsevier Limited and Science Press. All rights reserved.
doi: 10.1016/S1672-6529(16)60402-X

1 Introduction

Primate's eye is the most important organ for information acquisition. More than 80% information is obtained from eye. Eye can focus on target at the center of the retina (foveal area) even when the target changes drastically. This is significant for robots which often work in bumpy and unstructured environment. A robot equipped with bionic eye can work better in terms of perception and control[1–5]. Bionic eye's motion modes mainly include saccade, smooth pursuit, vergence, Vestibule-Ocular Reflex (VOR), Optokinetic Reflex (OKR) and eye-head coordination. Two most important motion modes for bionic eye are saccade and smooth pursuit. The current studies of saccade and smooth pursuit are mainly focused on the imitation based on visual neural feedback mechanism.

Saccade is used to move the eye's fixation point voluntarily from one point to another rapidly, which is significant for robots to select and change their regions of interest quickly. Saccade control system acts as a position servo controller to keep the target at the center of retina with minimum time consuming. Young and Stark[6] proposed a sampled data model for saccade. Its input is target position in retina or target angular position produced by optic nerve. The circuit of the model contains dead zone and INHBT (a device to inhibit the timing circuit). When the error exceeds a certain threshold, the pulse generator is triggered which causes a sample to be taken. Robinson[7] modified Young's model by adding premotor circuitry, which consists of Medial Longitudinal Fasciculus (MLF) and Neural Integrator (NI). Quaia *et al*.[8] proposed a new model for saccade based on the fact that the Superior Colliculus (SC) and the cerebellum are important to produce accurate saccadic movements. The superior colliculus provides a directional drive of eye movement while the cerebellum keeps tracking of the saccade toward target. The sum of the superior colliculus and the cerebellum is passed on to the motoneurons (MNs) and determines the eye's velocity. Chen-Harris *et al*.[9] found that in saccadic task, the brain relies on an internal feedback that has the

Corresponding author: De Xu
E-mail: de.xu@ia.ac.cn

characteristics of a fast-adapting forward model. Chao *et al*.[10] presented an ocular-motor development model that inspired by ideas and data from developmental psychology.

Smooth pursuit system acts as a velocity servo controller to rotate eye at the same angular rate as target while keeping it imaged at desired position or in desired region. In Robinson's model of smooth pursuit[11], the input is the velocity of target's image across the retina. The velocity deviation is taken as the major stimulus to pursuit, and it is transformed into an eye velocity command. Based on Robinson's model, Brown[12] added smith predictor to cope with the time delay. Deno *et al*.[13] applied dynamical neural network, which unifies two apparently disparate models of smooth pursuit and dynamical element organization to the smooth pursuit system. The dynamical neural network can compensate delays from sensory input to motor response. Lunghi *et al*.[14] introduced a neural adaptive predictor which is previously trained to accomplish smooth pursuit. This model can explain human's ability to compensate the 130 ms physiological delays when human beings follow the external targets with their eyes. Avni *et al*.[15] presented a framework for visual scanning and target tracking with a set of independent pan-tilt cameras based on Model Predictive Control (MPC). Zhang *et al*.[16] implemented smooth pursuit eye movement with prediction and learning as well as solving the problem of time delays in the visual pathways.

Besides, some saccade and smooth pursuit models have been validated on bionic eye systems[17–22]. Santini *et al*.[17] show that the oculomotor strategies by which humans scan visual scenes produce parallaxes that provide accurate estimation of distance. Chinellato *et al*.[18] realized coordinated control of eye and arm movements through configuration and training. Song and Zhang[19] proposed a binocular control model, which is derived from neural pathway, for saccade and smooth pursuit. In their smooth pursuit experiments, the maximum retinal error is less than 2.2 degrees, which can keep a target in the field of view accurately. Wang *et al*.[20] designed an active vision system which can imitate saccade and smooth pursuit. The saccadic movement is implemented with open-loop controller, which ensures faster saccade eye movement compared with closed-loop controller. Antonelli *et al*.[21] realized the saccadic movement on a robot head by using a model called Recurrent Architecture (RA). Wang *et al*.[22] developed an autonomous mobile manipulation system that using a modified Image-Based Visual Servo (IBVS) controller.

The works mentioned above are significant for the development of bionic eye. But there are some shortcomings for them. Firstly, most of the existing methods are based on the principle of neurology, whose further developments and applications may be limited by people's understanding to human eye. Secondly, only 2D image information is applied when saccade and smooth pursuit controls are implemented, while 3D information is ignored. Thirdly, most of these methods focus on monocular independent control and take little considerations for the coordinated control between two eyes, which results in the fact that the bionic eye's important role of 3D measurement through the binocular vision is ignored.

In order to overcome the shortcomings mentioned above in certain extent, a novel control method that implements the saccade and smooth pursuit according to 3D coordinates is proposed in this paper. A bionic eye system that consists of a visual sub-system and a motion sub-system is designed to fulfill the control method. Due to the characteristics of platform, optimal observation position and motion planning are developed. The optimal observation position is applied for the accurately acquisition of 3D coordinates. The response speed and running smoothness of motor can be improved with the using of motion planning. The saccade and smooth pursuit based on 3D coordinates can provide some references for the 3D reconstruction and 3D recognition of bionic eye.

The rest of the paper is organized as follows. In section **2**, the bionic eye platform is introduced and the control method is given. Section **3** gives the calculation of 3D coordinates. In section **4**, the optimal observation position is discussed and calculated. In section **5**, the motion planning method is developed. The experimental results are given and discussed in section **6** and finally conclusions are drawn in section **7**.

2 Platform and control system

2.1 Platform and coordinate system

Fig. 1 shows the mechanical structure of bionic eye and the coordinate systems of the bionic eye platform. It consists of vision sub-system and motion sub-system. The vision sub-system is composed by two CCD cam-

eras, which act as left eye and right eye. The motion sub-system includes four stepper motors and two motion modules that used to fix cameras. The yaw and pitch of every camera are controlled by two stepper motors respectively. The rotation axes of yaw and pitch are perpendicular and intersect. The camera's optical center and the rotation center are not coincident. $O_c^l X_c^l Y_c^l Z_c^l$ is the coordinate system of left camera, and $O_p^l X_p^l Y_p^l Z_p^l$ is the left motion module base coordinate system. The definitions of $O_c^r X_c^r Y_c^r Z_c^r$ and $O_p^r X_p^r Y_p^r Z_p^r$ are similar to those of left camera. $O_w X_w Y_w Z_w$ is the world coordinate system, whose O_w coincides with O_p^l, and its X_w, Y_w, Z_w are parallel to X_p^l, Y_p^l, Z_p^l respectively. In the initial position, the motion module end coordinate systems $O_e^l X_e^l Y_e^l Z_e^l$ and $O_e^r X_e^r Y_e^r Z_e^r$ coincide with their motion module base coordinate systems $O_p^l X_p^l Y_p^l Z_p^l$ and $O_p^r X_p^r Y_p^r Z_p^r$ respectively. $\boldsymbol{T}$ is the transformation matrix from $O_c^r X_c^r Y_c^r Z_c^r$ to $O_c^l X_c^l Y_c^l Z_c^l$. $\boldsymbol{T}_m^l$ is transformation matrix from $O_e^l X_e^l Y_e^l Z_e^l$ to $O_c^l X_c^l Y_c^l Z_c^l$, and $\boldsymbol{T}_m^r$ is transformation matrix from $O_e^r X_e^r Y_e^r Z_e^r$ to $O_c^r X_c^r Y_c^r Z_c^r$. $\boldsymbol{T}_m^l$ is transformation matrix from $O_w X_w Y_w Z_w$ to $O_p^l X_p^l Y_p^l Z_p^l$, and $\boldsymbol{T}_w^r$ is transformation matrix from $O_w X_w Y_w Z_w$ to $O_p^r X_p^r Y_p^r Z_p^r$.

2.2 Control system

Fig. 2 shows the block diagram of bionic eye control system, which combines saccade and smooth pursuit together. Two eyes' position and two images of left and right cameras are used for the 3D coordinates' calculation of target based on binocular stereo vision. A filter is used to estimate target's state when the target is moving. The calculated optimal observation position according to the 3D coordinates is the desired position of motor. The acceleration of motor can be derived by motion planning. Motor control is carried out based on the current velocity and acceleration. As a result, the variation of motor position is changed into the variation of eye.

3 3D coordinates calculation

3D coordinates are the basis of control model applied in this paper, and it can be gotten by combining with the image coordinates of target and the camera position. Fig. 3 shows the principle of 3D coordinates calculation. It is necessary to solve the following questions to ensure the realization of binocular stereo vision and motion control function. The first is the parameters including the intrinsic parameters of camera, eye-hand parameters and extrinsic parameters in initial location need to be off-line calibrated. The second is the image coordinates of target in left and right images need to be extracted in real-time. The third is 3D coordinates need to be calculated in real-time. The fourth is 3D coordinates in next cycle need to be predicted with a filter when the target is moving.

3.1 Parameters calibration

The intrinsic parameter matrices of the left and right cameras are obtained according to the calibration method in Ref. [23]. The distortion parameter matrices of the left and right cameras are calibrated using the model reported in Ref. [24]. The binocular extrinsic parameters are acquired by stereo calibration method.

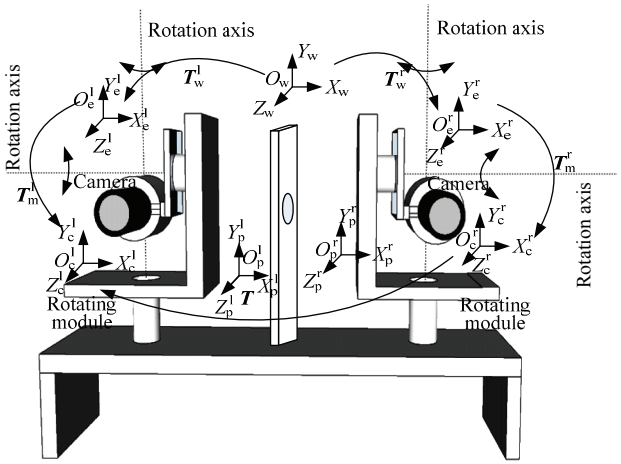

Fig. 1 The mechanical structure and coordinate systems of the bionic eye platform.

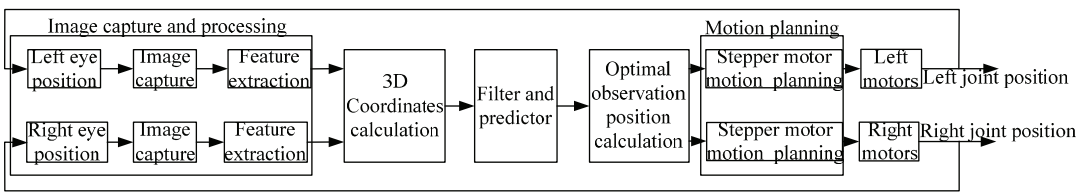

Fig. 2 The block diagram of bionic eye control system.

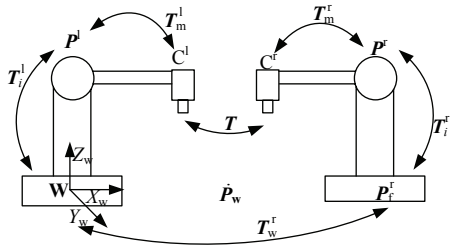

Fig. 3 The principle of 3D coordinates calculation.

In the bionic eye system, the motion module end can be regarded as the robot end. So, eye-hand calibration method can be used to calibrate the extrinsic parameters between the camera and motion module end. The eye-hand parameters of left and right eye are calibrated by the method in Ref. [25].

3.2 The feature extraction of target

A simple circular pattern target is used in this paper. In order to get the 3D coordinates of target, the coordinates of target's center in left and right images are extracted. Firstly, the images are binarized with a threshold. Secondly, all contours except some small contours in binary image are obtained. Thirdly, a contour is selected with the nearest distance to the predicted target center on image. Lastly, the contour's center is fitted based on the least-square ellipse fitting.

3.3 3D coordinates calculation

$(u^{\mathrm{l}}, v^{\mathrm{l}})$ and $(u^{\mathrm{r}}, v^{\mathrm{r}})$ are the target's image coordinates on the images of left and right cameras. $(x_{\mathrm{cl}}^{\mathrm{l}}, y_{\mathrm{cl}}^{\mathrm{l}})$ and $(x_{\mathrm{cl}}^{\mathrm{r}}, y_{\mathrm{cl}}^{\mathrm{r}})$ are the coordinates in left normalization image plane and right normalization image plane, respectively, and they are calculated as follows:

$$\begin{pmatrix} x_{\mathrm{cl}}^{\mathrm{l}} \\ y_{\mathrm{cl}}^{\mathrm{l}} \\ 1 \end{pmatrix} = \begin{pmatrix} f_x^{\mathrm{l}} & 0 & u_0^{\mathrm{l}} \\ 0 & f_y^{\mathrm{l}} & v_0^{\mathrm{l}} \\ 0 & 0 & 1 \end{pmatrix}^{-1} \begin{pmatrix} u^{\mathrm{l}} \\ v^{\mathrm{l}} \\ 1 \end{pmatrix}, \tag{1}$$

$$\begin{pmatrix} x_{\mathrm{cl}}^{\mathrm{r}} \\ y_{\mathrm{cl}}^{\mathrm{r}} \\ 1 \end{pmatrix} = \begin{pmatrix} f_x^{\mathrm{r}} & 0 & u_0^{\mathrm{r}} \\ 0 & f_y^{\mathrm{r}} & v_0^{\mathrm{r}} \\ 0 & 0 & 1 \end{pmatrix}^{-1} \begin{pmatrix} u^{\mathrm{r}} \\ v^{\mathrm{r}} \\ 1 \end{pmatrix}, \tag{2}$$

where $(f_{\mathrm{x}}^{\mathrm{l}}, y_{\mathrm{y}}^{\mathrm{l}})$ and $(f_{\mathrm{x}}^{\mathrm{r}}, y_{\mathrm{y}}^{\mathrm{r}})$ are magnification factors, $(u_0^{\mathrm{l}}, v_0^{\mathrm{l}})$ and $(u_0^{\mathrm{r}}, v_0^{\mathrm{r}})$ are image coordinates of the primary points of the left and right cameras.

$\boldsymbol{P}_{\mathrm{lc}}^{\mathrm{w}} = (x_{\mathrm{lc}}^{\mathrm{w}}, y_{\mathrm{lc}}^{\mathrm{w}}, z_{\mathrm{lc}}^{\mathrm{w}})$ and $\boldsymbol{P}_{\mathrm{rc}}^{\mathrm{w}} = (x_{\mathrm{rc}}^{\mathrm{w}}, y_{\mathrm{rc}}^{\mathrm{w}}, z_{\mathrm{rc}}^{\mathrm{w}})$ are the coordinates of $\boldsymbol{P}_{\mathrm{cl}}^{\mathrm{l}}$ and $\boldsymbol{P}_{\mathrm{cl}}^{\mathrm{r}}$ in the world coordinates system, respectively. They can be calculated as follows:

$$\boldsymbol{P}_{\mathrm{lc}}^{\mathrm{w}} = \mathrm{rot}(Y^{\mathrm{l}}, \theta^{\mathrm{l}})\mathrm{rot}(X^{\mathrm{l}}, \alpha^{\mathrm{l}})\boldsymbol{T}_{\mathrm{m}}^{\mathrm{l}} \begin{pmatrix} x_{\mathrm{cl}}^{\mathrm{l}} \\ y_{\mathrm{cl}}^{\mathrm{l}} \\ 1 \end{pmatrix}, \tag{3}$$

$$\boldsymbol{P}_{\mathrm{rc}}^{\mathrm{w}} = \mathrm{rot}(Y^{\mathrm{r}}, \theta^{\mathrm{r}})\mathrm{rot}(X^{\mathrm{r}}, \alpha^{\mathrm{r}})\boldsymbol{T}_{\mathrm{m}}^{\mathrm{r}} \begin{pmatrix} x_{\mathrm{cl}}^{\mathrm{r}} \\ y_{\mathrm{cl}}^{\mathrm{r}} \\ 1 \end{pmatrix}. \tag{4}$$

$\boldsymbol{P}_{\mathrm{l0}}^{\mathrm{w}} = (x_{\mathrm{l0}}^{\mathrm{w}}, y_{\mathrm{l0}}^{\mathrm{w}}, z_{\mathrm{l0}}^{\mathrm{w}})$ and $\boldsymbol{P}_{\mathrm{r0}}^{\mathrm{w}} = (x_{\mathrm{r0}}^{\mathrm{w}}, y_{\mathrm{r0}}^{\mathrm{w}}, z_{\mathrm{r0}}^{\mathrm{w}})$ are the coordinates of left and right cameras' optical center in the world coordinates system, respectively, and they can be obtained as follows:

$$\boldsymbol{P}_{\mathrm{l0}}^{\mathrm{w}} = \boldsymbol{T}_i^{\mathrm{l}}\boldsymbol{T}_{\mathrm{m}}^{\mathrm{l}} \begin{pmatrix} 0 \\ 0 \\ 1 \end{pmatrix}, \tag{5}$$

$$\boldsymbol{P}_{\mathrm{r0}}^{\mathrm{w}} = \boldsymbol{T}_i^{\mathrm{r}}\boldsymbol{T}_{\mathrm{m}}^{\mathrm{r}} \begin{pmatrix} 0 \\ 0 \\ 1 \end{pmatrix}. \tag{6}$$

The lines $\boldsymbol{P}_{\mathrm{l0}}^{\mathrm{w}}\boldsymbol{P}_{\mathrm{lc}}^{\mathrm{w}}$ and $\boldsymbol{P}_{\mathrm{r0}}^{\mathrm{w}}\boldsymbol{P}_{\mathrm{rc}}^{\mathrm{w}}$ can be derived as Eqs. (7) and (8), respectively. The intersection point of $\boldsymbol{P}_{\mathrm{l0}}^{\mathrm{w}}\boldsymbol{P}_{\mathrm{lc}}^{\mathrm{w}}$ and $\boldsymbol{P}_{\mathrm{r0}}^{\mathrm{w}}\boldsymbol{P}_{\mathrm{rc}}^{\mathrm{w}}$ can be calculated by solving Eqs. (7) and (8):

$$\frac{x - x_{\mathrm{l0}}^{\mathrm{w}}}{x_{\mathrm{ln}}^{\mathrm{w}} - x_{\mathrm{l0}}^{\mathrm{w}}} = \frac{y - y_{\mathrm{l0}}^{\mathrm{w}}}{y_{\mathrm{ln}}^{\mathrm{w}} - y_{\mathrm{l0}}^{\mathrm{w}}} = \frac{z - z_{\mathrm{l0}}^{\mathrm{w}}}{z_{\mathrm{ln}}^{\mathrm{w}} - z_{\mathrm{l0}}^{\mathrm{w}}}, \tag{7}$$

$$\frac{x - x_{\mathrm{r0}}^{\mathrm{w}}}{x_{\mathrm{rn}}^{\mathrm{w}} - x_{\mathrm{r0}}^{\mathrm{w}}} = \frac{y - y_{\mathrm{r0}}^{\mathrm{w}}}{y_{\mathrm{rn}}^{\mathrm{w}} - y_{\mathrm{r0}}^{\mathrm{w}}} = \frac{z - z_{\mathrm{r0}}^{\mathrm{w}}}{z_{\mathrm{rn}}^{\mathrm{w}} - z_{\mathrm{r0}}^{\mathrm{w}}}. \tag{8}$$

3.4 3D coordinates prediction

The 3D coordinates of target have a time delay for motor control when it is moving. A low-pass filter is used to eliminate the noises with high frequency in the 3D coordinates. The 3D coordinates in next control cycle can be predicted with the target's velocity and its current coordinates can be obtained as:

$$\begin{pmatrix} \overline{x}_{i+1} \\ \overline{y}_{i+1} \\ \overline{z}_{i+1} \end{pmatrix} = \begin{pmatrix} x_i + v_{xi}\Delta t \\ y_i + v_{yi}\Delta t \\ z_i + v_{zi}\Delta t \end{pmatrix}, \tag{9}$$

where (v_{xi}, v_{yi}, v_{zi}) is the target's velocity at i-th sampling, Δt is the control cycle time. (x_i, y_i, z_i) is the 3D coordinates at i-th sampling, $(\overline{x}_{i+1}, \overline{y}_{i+1}, \overline{z}_{i+1})$ is the predicted 3D coordinates at i+1-th sampling.

4 Optimal observation position

The optimal observation position is used for the accurate acquisition of 3D coordinates. The 3D coordinates' accuracy is related to baseline, time difference and image distortion. In the bionic eye platform, the baseline is changed with the changes of camera positions because the optical center is not coincident with the center of rotation. It is well known that the error of 3D coordinates of target is smaller when the baseline of two cameras is longer. So, it is necessary to keep the baseline unchanged. On the other hand, there is time difference caused by unstick synchronization between image acquisition and camera position acquisition. As shown in Fig.4a, the error of *z*-coordinate is much smaller with two cameras moving in the same direction than that two cameras moving in opposite direction (Fig. 4b). It is necessary to keep the target in the center areas of two camera's images in order to get accurate 3D coordinates of the target.

4.1 Optimal observation position

As shown in Fig. 5, $\boldsymbol{m}^{\mathrm{l}}$ and $\boldsymbol{m}^{\mathrm{r}}$ are the image coordinates of $\boldsymbol{P}_{\mathrm{w}}$ in left and right cameras respectively; $\boldsymbol{m}_{\mathrm{o}}^{\mathrm{l}}$ and $\boldsymbol{m}_{\mathrm{o}}^{\mathrm{r}}$ are the image centers of left and right cameras respectively. $\boldsymbol{P}^{\mathrm{l}}$ is the vertical point of $\boldsymbol{P}_{\mathrm{w}}$ to the line of $O_{\mathrm{c}}^{\mathrm{l}}Z_{\mathrm{c}}^{\mathrm{l}}$ and $\boldsymbol{P}^{\mathrm{r}}$ is the vertical point of $\boldsymbol{P}_{\mathrm{w}}$ to the line of $O_{\mathrm{c}}^{\mathrm{r}}Z_{\mathrm{c}}^{\mathrm{r}}$. Δm^{l} is the distance between $\boldsymbol{m}^{\mathrm{l}}$ and $\boldsymbol{m}_{\mathrm{o}}^{\mathrm{l}}$. Δm^{r} is the distance between $\boldsymbol{m}^{\mathrm{r}}$ and $\boldsymbol{m}_{\mathrm{o}}^{\mathrm{r}}$. D_{b} is the length of baseline. The pitch angles of left and right cameras in optimal observation position are α^{l} and α^{r} respectively. The yaw angles of left and right cameras in optimal observation position are θ^{l} and θ^{r} respectively. $\boldsymbol{P}_{\mathrm{ob}}(\alpha^{\mathrm{l}}, \theta^{\mathrm{l}}, \alpha^{\mathrm{r}}, \theta^{\mathrm{r}})$ is the optimal observation position. The thresholds of Δm^{l} and Δm^{r} are γ^{l} and γ^{r}, which can be set based on the image distortion radius.

The optimal observation position need meet the conditions listed as in Eq. (10). When the target is very closer with eyes, whose optimal observation position cannot be obtained, the image position of target can be kept at the image center. It is difficult to obtain the optimal solution of optimal observation position based on the Eq. (10). But a suboptimal solution can be obtained by using a simplified calculation method. α_i^{l} and α_i^{r} are calculated in the case that θ_i^{l} and θ_i^{r} are equal to zero at first, and then, θ_i^{l} and θ_i^{r} are calculated while α_i^{l} and α_i^{r} are kept equal to the calculated value and unchanged. Trial and error method can be used to get the optimal

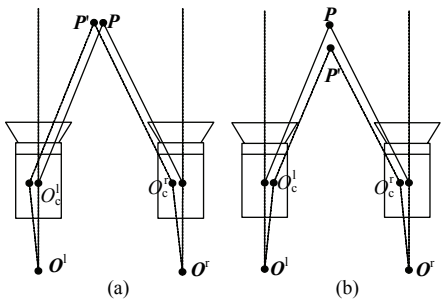

Fig. 4 The sketch map of *z*-coordinate's error (***P***–***P***') generated by time difference between the image acquisitions. (a) Two cameras moving in the same direction; (b) two cameras moving in the opposite direction.

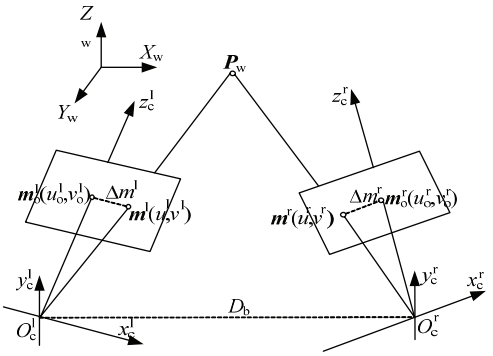

Fig. 5 The sketch map of relationship between a Cartesian point and its image point.

solution when suboptimal solution is obtained. The range of α is from α_{lth} to α_{hth} and the range of θ is from θ_{lth} to θ_{hth}.

$$\begin{cases} \alpha^{\mathrm{l}} = \alpha^{\mathrm{r}} = \alpha \\ \theta^{\mathrm{l}} = \theta^{\mathrm{r}} = \theta \\ \Delta m^{\mathrm{l}} = -\Delta m^{\mathrm{r}} \end{cases}. \tag{10}$$

4.2 Calculation of α^{l} and α^{r}

As mentioned above, $\boldsymbol{P}_{\mathrm{c}}^{\mathrm{l}}$ and $\boldsymbol{P}_{\mathrm{c}}^{\mathrm{r}}$ are the coordinates in left and right camera coordinate systems of $\boldsymbol{P}_{\mathrm{w}}$. $\boldsymbol{P}_{\mathrm{c}}^{\mathrm{l}}$ and $\boldsymbol{P}_{\mathrm{c}}^{\mathrm{r}}$ can be obtained by Eqs. (11) and (13). $\boldsymbol{T}_{\mathrm{w}}^{\mathrm{l}}$ and $\boldsymbol{T}_{\mathrm{c}}^{\mathrm{r}}$ are the transformation matrices between world coordinate system and motion module base coordinate system:

$$\boldsymbol{P}_{\mathrm{c}}^{\mathrm{l}} = (\boldsymbol{T}_{\mathrm{m}}^{\mathrm{l}})^{-1}(\boldsymbol{T}_{\mathrm{x}}^{\mathrm{l}})^{-1}(\boldsymbol{T}_{\mathrm{w}}^{\mathrm{l}})^{-1}\boldsymbol{P}_{\mathrm{w}}, \tag{11}$$

where

$$(\boldsymbol{T}_{\mathrm{m}}^{\mathrm{l}})^{-1} = \begin{pmatrix} n_x^{\mathrm{l}} & o_x^{\mathrm{l}} & a_x^{\mathrm{l}} & p_x^{\mathrm{l}} \\ n_y^{\mathrm{l}} & o_y^{\mathrm{l}} & a_y^{\mathrm{l}} & p_y^{\mathrm{l}} \\ n_z^{\mathrm{l}} & o_z^{\mathrm{l}} & a_z^{\mathrm{l}} & p_z^{\mathrm{l}} \\ 0 & 0 & 0 & 1 \end{pmatrix}, \tag{12}$$

$$\boldsymbol{P}_{\mathrm{c}}^{\mathrm{r}}=(\boldsymbol{T}_{\mathrm{m}}^{\mathrm{r}})^{-1}(\boldsymbol{T}_{\mathrm{x}}^{\mathrm{r}})^{-1}(\boldsymbol{T}_{\mathrm{w}}^{\mathrm{r}})^{-1}\boldsymbol{P}_{\mathrm{w}}, \tag{13}$$

where

$$(\boldsymbol{T}_{\mathrm{m}}^{\mathrm{r}})^{-1}=\begin{pmatrix} n_x^{\mathrm{r}} & o_x^{\mathrm{r}} & a_x^{\mathrm{r}} & p_x^{\mathrm{r}} \\ n_y^{\mathrm{r}} & o_y^{\mathrm{r}} & a_y^{\mathrm{r}} & p_y^{\mathrm{r}} \\ n_z^{\mathrm{r}} & o_z^{\mathrm{r}} & a_z^{\mathrm{r}} & p_z^{\mathrm{r}} \\ 0 & 0 & 0 & 1 \end{pmatrix}. \tag{14}$$

In order to simplify the calculation, Eqs. (15) and (16) are gotten:

$$\boldsymbol{P}_{\mathrm{w}}^{\mathrm{l}}=(\boldsymbol{T}_{\mathrm{w}}^{\mathrm{l}})^{-1}\boldsymbol{P}_{\mathrm{w}}, \tag{15}$$

$$\boldsymbol{P}_{\mathrm{w}}^{\mathrm{r}}=(\boldsymbol{T}_{\mathrm{w}}^{\mathrm{r}})^{-1}\boldsymbol{P}_{\mathrm{w}}. \tag{16}$$

The image coordinate deviation between the coordinate of target and image center can be obtained as follows:

$$\begin{pmatrix}\Delta u^{\mathrm{l}}\\ \Delta v^{\mathrm{l}}\end{pmatrix}=\begin{pmatrix}u^{\mathrm{l}}\\ v^{\mathrm{l}}\end{pmatrix}-\begin{pmatrix}u_0^{\mathrm{l}}\\ v_0^{\mathrm{l}}\end{pmatrix}, \tag{17}$$

$$\begin{pmatrix}\Delta u^{\mathrm{r}}\\ \Delta v^{\mathrm{r}}\end{pmatrix}=\begin{pmatrix}u^{\mathrm{r}}\\ v^{\mathrm{r}}\end{pmatrix}-\begin{pmatrix}u_0^{\mathrm{r}}\\ v_0^{\mathrm{r}}\end{pmatrix}. \tag{18}$$

So, Eqs. (19) and (20) can be derived by combined with Eqs. (11) to (18):

$$\begin{cases}\Delta u^{\mathrm{l}}=\\ f_x^{\mathrm{l}}\dfrac{(o_x^{\mathrm{l}}y_w^{\mathrm{l}}+a_x^{\mathrm{l}}z_w^{\mathrm{l}})\cos\alpha+(o_x^{\mathrm{l}}z_w^{\mathrm{l}}-a_x^{\mathrm{l}}y_w^{\mathrm{l}})\sin\alpha+(p_x^{\mathrm{l}}+n_x^{\mathrm{l}}x_w^{\mathrm{l}})}{(o_z^{\mathrm{l}}y_w^{\mathrm{l}}+a_z^{\mathrm{l}}z_w^{\mathrm{l}})\cos\alpha+(o_z^{\mathrm{l}}z_w-a_z^{\mathrm{l}}y_w^{\mathrm{l}})\sin\alpha+(p_z^{\mathrm{l}}+n_z^{\mathrm{l}}x_w^{\mathrm{l}})},\\ \Delta v^{\mathrm{l}}=\\ f_y^{\mathrm{l}}\dfrac{(o_y^{\mathrm{l}}y_w^{\mathrm{l}}+a_y^{\mathrm{l}}z_w^{\mathrm{l}})\cos\alpha+(o_y^{\mathrm{l}}z_w^{\mathrm{l}}-a_y^{\mathrm{l}}y_w^{\mathrm{l}})\sin\alpha+(p_y^{\mathrm{l}}+n_y^{\mathrm{l}}x_w^{\mathrm{l}})}{(o_z^{\mathrm{l}}y_w^{\mathrm{l}}+a_z^{\mathrm{l}}z_w^{\mathrm{l}})\cos\alpha+(o_z^{\mathrm{l}}z_w^{\mathrm{l}}-a_z^{\mathrm{l}}y_w^{\mathrm{l}})\sin\alpha+(p_z^{\mathrm{l}}+n_z^{\mathrm{l}}x_w^{\mathrm{l}})}\end{cases}, \tag{19}$$

$$\begin{cases}\Delta u^{\mathrm{r}}=\\ f_x^{\mathrm{r}}\dfrac{(o_x^{\mathrm{r}}y_w^{\mathrm{r}}+a_x^{\mathrm{r}}z_w^{\mathrm{r}})\cos\alpha+(o_x^{\mathrm{r}}z_w^{\mathrm{r}}-a_x^{\mathrm{r}}y_w^{\mathrm{r}})\sin\alpha+(p_x^{\mathrm{r}}+n_x^{\mathrm{r}}x_w^{\mathrm{r}})}{(o_z^{\mathrm{r}}y_w^{\mathrm{r}}+a_z^{\mathrm{r}}z_w^{\mathrm{r}})\cos\alpha+(o_z^{\mathrm{r}}z_w-a_z^{\mathrm{r}}y_w^{\mathrm{r}})\sin\alpha+(p_z^{\mathrm{r}}+n_z^{\mathrm{r}}x_w^{\mathrm{r}})},\\ \Delta v^{\mathrm{r}}=\\ f_y^{\mathrm{r}}\dfrac{(o_y^{\mathrm{r}}y_w^{\mathrm{r}}+a_y^{\mathrm{r}}z_w^{\mathrm{r}})\cos\alpha+(o_y^{\mathrm{r}}z_w^{\mathrm{r}}-a_y^{\mathrm{r}}y_w^{\mathrm{r}})\sin\alpha+(p_y^{\mathrm{r}}+n_y^{\mathrm{r}}x_w^{\mathrm{r}})}{(o_z^{\mathrm{r}}y_w^{\mathrm{r}}+a_z^{\mathrm{r}}z_w^{\mathrm{r}})\cos\alpha+(o_z^{\mathrm{r}}z_w^{\mathrm{r}}-a_z^{\mathrm{r}}y_w^{\mathrm{r}})\sin\alpha+(p_z^{\mathrm{r}}+n_z^{\mathrm{r}}x_w^{\mathrm{r}})}\end{cases}. \tag{20}$$

In order to get the solution of α which ensures the target is kept in the center area of two camera images, the solution of α need meet the conditions as listed in Eq. (22) and minimize E_{sv}. E_{sv} is expressed as:

$$E_{\mathrm{sv}}=\left|\Delta v^{\mathrm{l}}\right|+\left|\Delta v^{\mathrm{r}}\right|, \tag{21}$$

$$\begin{cases}\Delta v^{\mathrm{l}}+\Delta v^{\mathrm{r}}=0\\ \alpha_{\mathrm{lth}}\le\alpha\le\alpha_{\mathrm{hth}}\end{cases}. \tag{22}$$

Eq. (23) can be derived based on the Eqs. (19) to (22):

$$k_1\cos^2\alpha+k_2\sin^2\alpha+k_3\sin\alpha\cos\alpha+k_4\cos\alpha+k_5\sin\alpha+k_6=0, \tag{23}$$

where

$$k_1=f_y^{\mathrm{l}}(o_y^{\mathrm{l}}y_w^{\mathrm{l}}+a_y^{\mathrm{l}}z_w^{\mathrm{l}})(o_z^{\mathrm{r}}y_w^{\mathrm{r}}+a_z^{\mathrm{r}}z_w^{\mathrm{r}})+f_y^{\mathrm{r}}(o_z^{\mathrm{l}}y_w^{\mathrm{l}}+a_z^{\mathrm{l}}z_w^{\mathrm{l}})(o_y^{\mathrm{r}}y_w^{\mathrm{r}}+a_y^{\mathrm{r}}z_w^{\mathrm{r}}), \tag{24}$$

$$k_2=f_y^{\mathrm{l}}(o_y^{\mathrm{l}}z_w^{\mathrm{l}}-a_y^{\mathrm{l}}y_w^{\mathrm{l}})(o_z^{\mathrm{r}}z_w^{\mathrm{r}}-a_z^{\mathrm{r}}y_w^{\mathrm{r}})+f_y^{\mathrm{r}}(o_z^{\mathrm{l}}z_w^{\mathrm{l}}-a_z^{\mathrm{l}}y_w^{\mathrm{l}})(o_y^{\mathrm{r}}z_w^{\mathrm{r}}-a_y^{\mathrm{r}}y_w^{\mathrm{r}}), \tag{25}$$

$$k_3=f_y^{\mathrm{l}}(o_y^{\mathrm{l}}y_w^{\mathrm{l}}+a_y^{\mathrm{l}}z_w^{\mathrm{l}})(o_z^{\mathrm{r}}z_w^{\mathrm{r}}-a_z^{\mathrm{r}}y_w^{\mathrm{r}})+f_y^{\mathrm{l}}(o_y^{\mathrm{l}}z_w^{\mathrm{l}}-a_y^{\mathrm{l}}y_w^{\mathrm{l}})(o_z^{\mathrm{r}}y_w^{\mathrm{r}}+a_z^{\mathrm{r}}z_w^{\mathrm{r}})+f_y^{\mathrm{r}}(o_z^{\mathrm{l}}y_w^{\mathrm{l}}+a_z^{\mathrm{l}}z_w^{\mathrm{l}})(o_y^{\mathrm{r}}z_w^{\mathrm{r}}-a_y^{\mathrm{r}}y_w^{\mathrm{r}})+f_y^{\mathrm{r}}(o_z^{\mathrm{l}}z_w^{\mathrm{l}}-a_z^{\mathrm{l}}y_w^{\mathrm{l}})(o_y^{\mathrm{r}}y_w^{\mathrm{r}}+a_y^{\mathrm{r}}z_w^{\mathrm{r}}), \tag{26}$$

$$k_4=f_y^{\mathrm{l}}(o_y^{\mathrm{l}}y_w^{\mathrm{l}}+a_y^{\mathrm{l}}z_w^{\mathrm{l}})(p_z^{\mathrm{r}}+n_z^{\mathrm{r}}x_w^{\mathrm{r}})+f_y^{\mathrm{l}}(p_y^{\mathrm{l}}+n_y^{\mathrm{l}}x_w^{\mathrm{l}})(o_z^{\mathrm{r}}y_w^{\mathrm{r}}+a_z^{\mathrm{r}}z_w^{\mathrm{r}})+f_y^{\mathrm{r}}(o_z^{\mathrm{l}}y_w^{\mathrm{l}}+a_z^{\mathrm{l}}z_w^{\mathrm{l}})(p_y^{\mathrm{r}}+n_y^{\mathrm{r}}x_w^{\mathrm{r}})+f_y^{\mathrm{r}}(p_z^{\mathrm{l}}+n_z^{\mathrm{l}}x_w^{\mathrm{l}})(o_y^{\mathrm{r}}y_w^{\mathrm{r}}+a_y^{\mathrm{r}}z_w^{\mathrm{r}}), \tag{27}$$

$$k_5=f_y^{\mathrm{l}}(o_y^{\mathrm{l}}z_w^{\mathrm{l}}-a_y^{\mathrm{l}}y_w^{\mathrm{l}})(p_z^{\mathrm{r}}+n_z^{\mathrm{r}}x_w^{\mathrm{r}})+f_y^{\mathrm{l}}(p_y^{\mathrm{l}}+n_y^{\mathrm{l}}x_w^{\mathrm{l}})(o_z^{\mathrm{r}}z_w^{\mathrm{r}}-a_z^{\mathrm{r}}y_w^{\mathrm{r}})+f_y^{\mathrm{r}}(o_z^{\mathrm{l}}z_w^{\mathrm{l}}-a_z^{\mathrm{l}}y_w^{\mathrm{l}})(p_y^{\mathrm{r}}+n_y^{\mathrm{r}}x_w^{\mathrm{r}})+f_y^{\mathrm{r}}(p_z^{\mathrm{l}}+n_z^{\mathrm{l}}x_w^{\mathrm{l}})(o_y^{\mathrm{r}}z_w^{\mathrm{r}}-a_y^{\mathrm{r}}y_w^{\mathrm{r}}). \tag{28}$$

$$k_6=f_y^{\mathrm{l}}(p_y^{\mathrm{l}}+n_y^{\mathrm{l}}x_w^{\mathrm{l}})(p_z^{\mathrm{r}}+n_z^{\mathrm{r}}x_w^{\mathrm{r}})+f_y^{\mathrm{r}}(p_z^{\mathrm{l}}+n_z^{\mathrm{l}}x_w^{\mathrm{l}})(p_y^{\mathrm{r}}+n_y^{\mathrm{r}}x_w^{\mathrm{r}}). \tag{29}$$

cosα can be replaced by sinα. So, Eq. (30) can be obtained:

$$[(k_2-k_1)^2+k_3^2]\sin^4\alpha+[(k_2-k_1)^2+k_3^2]\sin^3\alpha+[2(k_2-k_1)k_6+k_5^2+k_4^2-k_3^2]\sin^2\alpha+[2k_5k_6-2k_3k_4]\sin\alpha+k_6^2-k_4^2=0. \tag{30}$$

The unique solution can be calculated by combined with Eqs. (22) and (30). If there is no solution, it shows that eyes cannot reach the optimal observation position and a neck will be needed.

4.3 Calculation of θ^{l} and θ^{r}

The calculations of θ^{l} and θ^{r} are the same as α^{l} and α^{r}. The calculation of Eqs. (31) and (32) is similar to the

calculations of α^{l} and α^{r} as follows:

$$\boldsymbol{P}_{c}^{l}=(\boldsymbol{T}_{m}^{l})^{-1}(\boldsymbol{T}_{x}^{l})^{-1}(\boldsymbol{T}_{y}^{l})^{-1}(\boldsymbol{T}_{w}^{l})^{-1}\boldsymbol{P}_{w}, \tag{31}$$

$$\boldsymbol{P}_{c}^{r}=(\boldsymbol{T}_{m}^{r})^{-1}(\boldsymbol{T}_{x}^{r})^{-1}(\boldsymbol{T}_{y}^{l})^{-1}(\boldsymbol{T}_{w}^{r})^{-1}\boldsymbol{P}_{w}, \tag{32}$$

where

$$\boldsymbol{T}_{x}^{l}=\mathrm{rot}(\mathrm{X}^{l},\alpha^{l}), \tag{33}$$

$$\boldsymbol{T}_{x}^{r}=\mathrm{rot}(\mathrm{X}^{r},\alpha^{r}). \tag{34}$$

The unique solution of θ can be obtained as the-same as α. The results of $\boldsymbol{P}_{ob}$ (α^{l}, θ^{l}, α^{r}, θ^{r}) are the desired positions in motion planning.

5 Motion planning

When optimal observation position is obtained, two cameras need to be controlled to the position by four stepper motors with desired angular velocity in schedule time. Then, two cameras can capture images at optimal observation position with the same velocity as target. Four motors use same control strategy, which is divided into two steps. The first is that the angular velocity of target (ω_s) is predicted based on angular deviation ($\Delta\theta$) between desired angle (θ_{sT}) and current angle (θ_0). It can be obtained by Eq. (35):

$$\omega_s=\frac{\Delta\theta}{T_0}. \tag{35}$$

where T_0 is an image processing cycle. The target is assumed to be uniform motion in current control cycle.

The second is the motion parameters are planned. The sketch map of motion planning is shown in Fig. 6. Fig. 6a shows the curves of angle, and Fig. 6b shows the curves of angle velocity. ω_{max} is the maximum angular velocity. In the bionic eye system, ω_{max} cannot be reached because the angle that the motor can reach is very small. Fig. 6c is a special case of Fig. 6b. In this case, the motion planning becomes simple. The stepper motor is controlled with the motion parameters, which consist of the acceleration of first stage (ε_1), the acceleration of second stage (ε_2), turning time (t_t) and the time that motor reaches the target position with the target's angular velocity (T), moving to given position with desired angular velocity in schedule time.

ε_1, ε_2 and the maximum acceleration of stepper motor, ε_{max} satisfy the Eq. (36):

$$|\varepsilon_1|,|\varepsilon_2|\le\varepsilon_{max}. \tag{36}$$

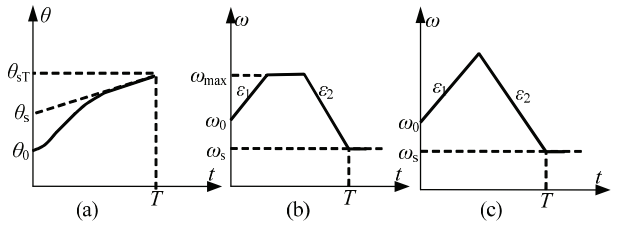

Fig. 6 The sketch map of motion planning. (a) Angle curves; (b) angle velocity curves; (c) a special case of (b).

So, Eqs. (37) to (39) can be derived as:

$$\Delta\theta+\omega_s T=\omega_0 t_t+\frac{1}{2}\varepsilon_1 t_t^2+(\omega_0+\varepsilon_1 t_t)(T-t_t)+\frac{1}{2}\varepsilon_2(T-t_t)^2, \tag{37}$$

$$\omega_s=\omega_0+\varepsilon_1 t_t+\varepsilon_2(T-t_t) \tag{38}$$

$$T\ge T_0 \tag{39}$$

where ω_0 is the current angular velocity of motor. In order to simplify the calculation, ε_1 can be assigned as:

$$\begin{cases}\varepsilon_1=\varepsilon_{max}, & \Delta\theta>(\omega_0-\omega_s)T_0\\ \varepsilon_1=0, & \Delta\theta>(\omega_0-\omega_s)T_0\\ \varepsilon_1=-\varepsilon_{max}, & \Delta\theta>(\omega_0-\omega_s)T_0\end{cases}. \tag{40}$$

In order to get the solutions of t_t, T and ε_2, the solving process is divided into 2 steps. In first step, T is set as T_0 and the solutions of t_t and ε_2 are calculated in term of the Eqs. (41) to (43).

$$t_t=\frac{2\Delta\theta-T_0(\omega_s-\omega_0)}{\varepsilon_1 T_0-\omega_s+\omega_0} \tag{41}$$

$$\varepsilon_2=\frac{\omega_s-\omega_0-\varepsilon_1 t_t}{T_0-t_t}, \tag{42}$$

$$t_t\ge 0. \tag{43}$$

When the solutions obtained from Eq. (41) are less than zero, Eq. (44) is derived:

$$\varepsilon_2=-\varepsilon_1. \tag{44}$$

Then, the solutions of t_t based on the Eqs. (37) and (38) are shown in Eqs. (45) and (46):

$$t_1=\frac{\omega_s-\omega_0-\sqrt{0.5(\omega_0^2+\omega_s^2)+\varepsilon_1\Delta\theta}}{\varepsilon_1}, \tag{45}$$

$$t_2=\frac{\omega_s-\omega_0+\sqrt{0.5(\omega_0^2+\omega_s^2)+\varepsilon_1\Delta\theta}}{\varepsilon_1}. \tag{46}$$

The unique solution of t_t can be obtained combined with Eqs. (43) and (47):

$$t_t = \min(t_1, t_2). \tag{47}$$

Then, T can be obtained as:

$$T = \frac{2\varepsilon_1 t_t + \omega_0 - \omega_s}{\varepsilon_1}. \tag{48}$$

The pulse number and frequency for the stepper motor can be gotten from the angular velocity.

6 Experiments and discussion

6.1 Experiment platform

A bionic eyes platform, which adopts a fixed mechatronic head, is used to imitate the motion mode of eyes. Two cameras with a resolution of 400 × 300 pixels are fixed on the head. Each camera can actively yaw and pitch driven by two independent stepper motors. The four motors' positions are obtained by four encoders. Compared with most existing bionic eye platforms that employ precise electronics as well as mechanism with high cost, the off-the-shelf cameras and common motors, which are more suitable for both the laboratory studies and industrialization, are applied for this bionic eye system.

The target is fixed on the manipulator of a KUKA robot so that the continuous and smooth motion can be guaranteed. The target is in front of the bionic eye platform. Fig. 7a shows the bionic eye system. Fig. 7b shows the target.

6.2 Saccade experiment

Saccade is used to move eyes voluntarily from one point to another, which can shifts fixation point quickly. During the saccadic experiments, the target is static while the cameras move from initial position to optimal observation position. The 3D coordinates obtained with the bionic eye vary with the cameras' motion, which will affect the result of optimal observation position. So, a position threshold is set to avoid the fluctuation of motor around the target position. Therefore, the optimal observation position calculated based on the method above is a suboptimal position that can satisfy the demand.

Figs. 8–10 show the result of saccade by using the motion planning and optimal observation position. Fig. 8 is the result on image plane. Figs. 8a and 8b show u and v coordinates of the target on left image respectively, and Figs. 8c and 8d show u and v coordinates of the target on right image respectively. The desired image coordinates are re-calculated based on the optimal observation position. The result of motors' position is shown in Fig. 9. Figs. 9a–9d show the positions of yaw motor of left eye, pitch motor of left eye, yaw motor of right eye and pitch motor of right eye, respectively. The desired position in Fig. 9 is the optimal observation position. The 3D coordinates of target when the bionic eye is moving are shown in Fig. 10. Fig. 10a is the results of 3D coordinates, and Figs. 10b, 10c and 10d show the result of x, y and z coordinates, respectively. The real value in Fig. 10 is obtained via manual measurement. Figs. 11a–11c show the error curves of image coordinates, motor positions and 3D coordinates of target, respectively. The results

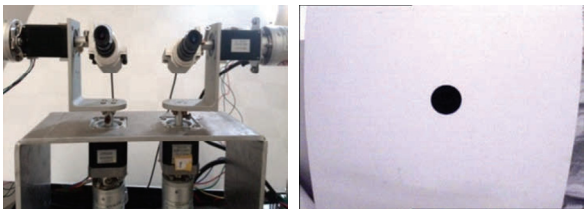

(a) (b)

Fig. 7 The bionic eye platform and target. (a) The bionic eye platform; (b) the target.

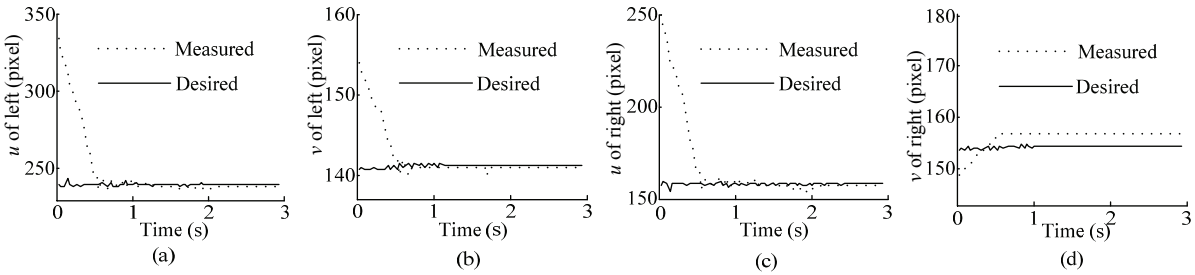

Fig. 8 The target's image coordinates in saccade when the optimal observation position and motion planning are used. (a) u-coordinates of target on left image; (b) v-coordinates of target on left image; (c) u-coordinates of target on right image; (d) v-coordinates of target on right image.

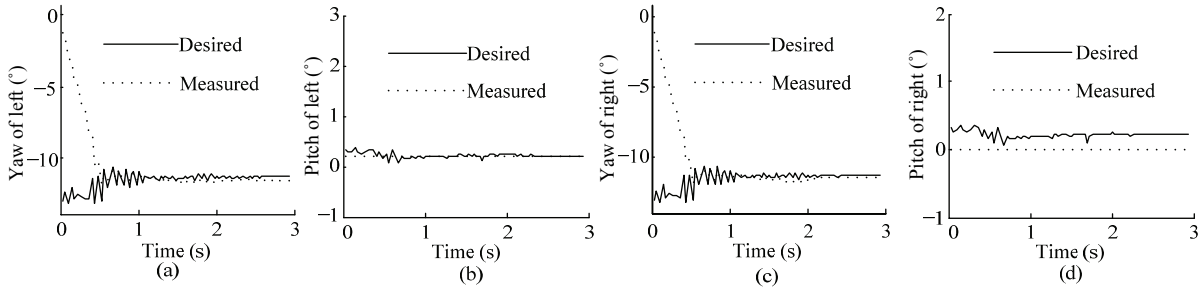

Fig. 9 The stepper motors' positions in saccade when the optimal observation position and motion planning are used. (a) Yaw angle of left camera; (b) pitch angle of left camera; (c) yaw angle of right camera; (d) pitch angle of right camera.

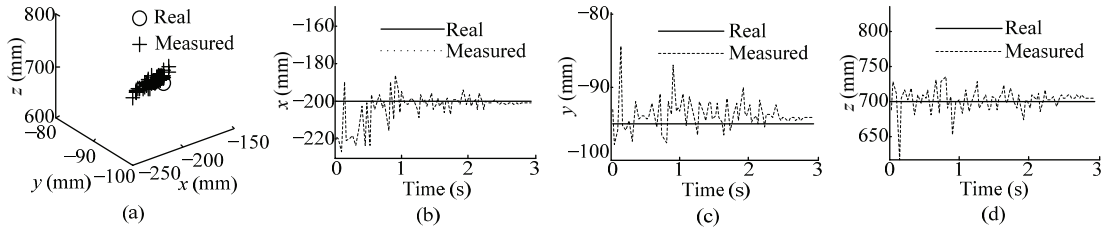

Fig. 10 The target's 3D coordinates in saccade when the optimal observation position and motion planning are used. (a) *xyz*-coordinates; (b) *x*-coordinates; (c) *y*-coordinates; (d) *z*-coordinates.

of comparative experiments are shown in Figs. 12–15. In the comparative experiments, eyes are controlled to keep the target at the centers of left image and right image without motion planning.

As shown in experimental results, some phenomena can be found. First, the time of eyes stabilizing at the desired position from initial position is reduced by using the motion planning. Figs. 8 and 9 show that the eyes are controlled to desired position in about 0.6 s. On the other hand, the time of comparative experiments is about 1.3 s. This is consistent with the purpose of motion planning. The result of motion planning is to make the stepper motor reach the desired position with least time. Second, the overshoot and waves are smaller when the stepper motor is controlled with motion planning. The overshoots of image coordinates and motor positions are approximately equal to zero in Figs. 8 and 9, while the overshoots of comparative experiments are more than 10% of desired position. Motor tracks are determined by motion planning, which avoids the overshoot. Third, the 3D coordinates obtained with the optimal observation position and motion planning is more accurate. Fig. 11c shows that the swing of coordinate's error is smaller than the result of Fig. 15c. What's more, the 3D coordinates obtained in optimal observation position are much closer to actual values than ones in comparative experiments. Fourth, Fig. 8 shows that the eyes can be controlled to keep the target at the center area of eyes. Finally, the computed 3D coordinates are unstable when the bionic eye is moving. This may mainly caused by the factors such as the angle acquisition error, the image resolution, the image distortion, the image feature extraction error, the time asynchronous and the calibration errors. With the development of technology and the more accurate device, these errors can be reduced.

Some conclusion can be obtained from above analysis. Saccade of bionic eye can be accomplished based on 3D coordinates; the 3D coordinates' accuracy can be improved by using optimal observation position; the motion planning can make the stepper motor move to desired position in least time with minimum overshoot.

6.3 Smooth pursuit experiment

Smooth pursuit is applied to track targets that move slowly. During the smooth pursuit experiments, the target is set at the end-effector of a KUKA robot to be moved from one point to another point in the horizontal direction. The velocity of target is 0.24 $m \cdot s^{-1}$. This experiment imitates that the bionic eye finds the target and tracks it. A filter is used for the position prediction of the target.

Fig. 16 shows the results of smooth pursuit experiment. In this experiment, the optimal observation position and motion planning are used. In comparative

experiment, the optimal observation position and motion planning are not used. Fig. 17 shows the results of the comparative experiment. Fig. 16a and Fig. 17a are the error curves of image coordinates. The errors are obtained from the desired image coordinates and measured coordinates. Figs. 16b–16d are 3D coordinates obtained by the method of this paper when the bionic eye is moving. Correspondingly, Figs. 17b–17d are the 3D coordinates of the comparative experiment.

As experiment result shown, the smooth pursuit can be accomplished with the proposed method in this paper. The image error can be kept at ± 20 pixels. The fluctuations of 3D coordinates are smaller when the optimal observation position and motion planning are used.

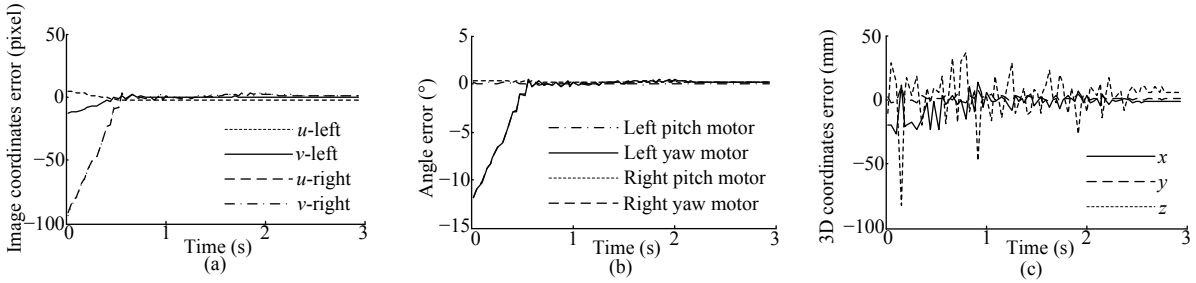

Fig. 11 Error curves in saccade when the optimal observation position and motion planning are used. (a) Image coordinates error; (b) stepper motors' positions error; (c) 3D coordinates error.

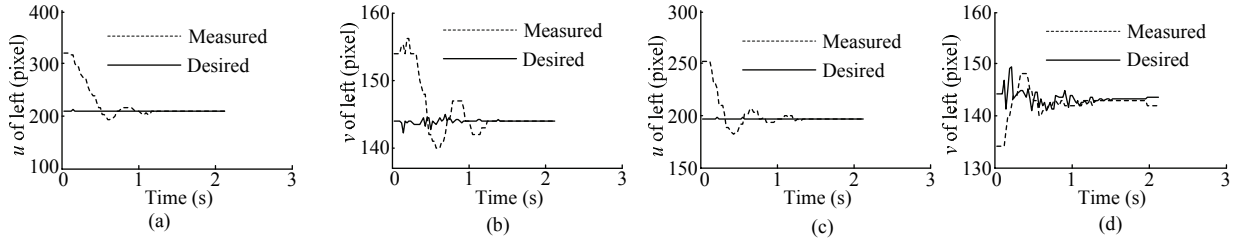

Fig. 12 The target's image coordinates in saccade when the optimal observation position and motion planning are not used. (a) *u*-coordinates of target on left image; (b) *v*-coordinates of target on left image; (c) *u*-coordinates of target on right image; (d) *v*-coordinates of target on right image.

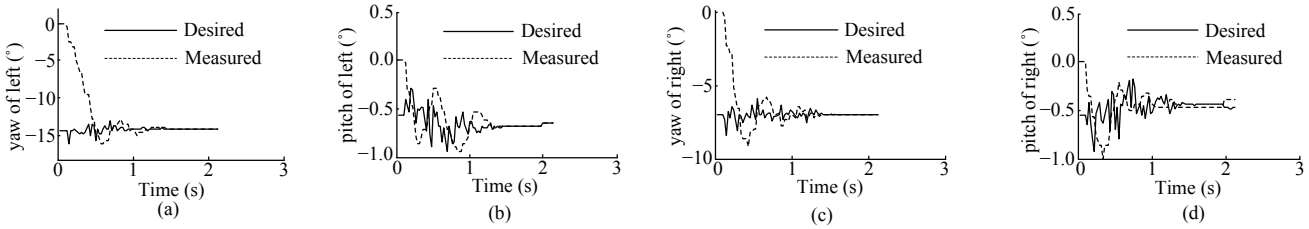

Fig. 13 The stepper motors' positions in saccade when the optimal observation position and motion planning are not used. (a) Yaw angle of left camera; (b) pitch angle of left camera; (c) yaw angle of right camera; (d) pitch angle of right camera.

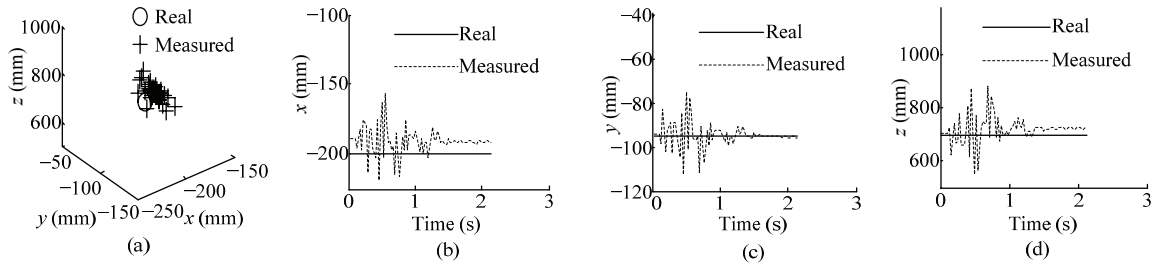

Fig. 14 The target's 3D coordinates in saccade when the optimal observation position and motion planning are not used. (a) *xyz*-coordinates; (b) *x*-coordinates; (c) *y*-coordinates; (d) *z*-coordinates.

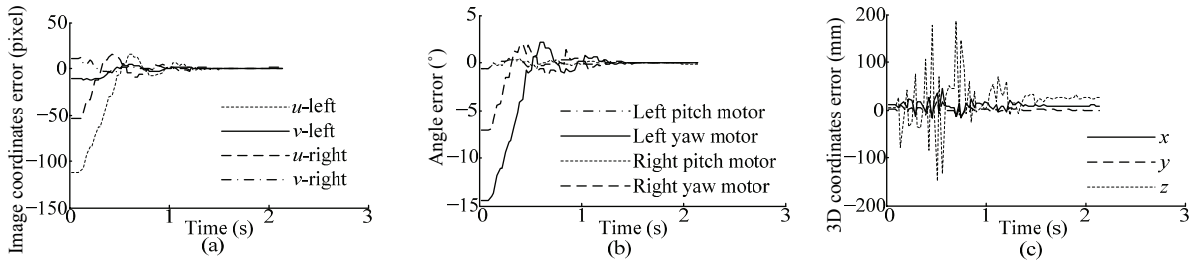

Fig. 15 Error curves in saccade when the optimal observation position and motion planning are used. (a) Image coordinates error; (b) stepper motors' positions error; (c) 3D coordinates error.

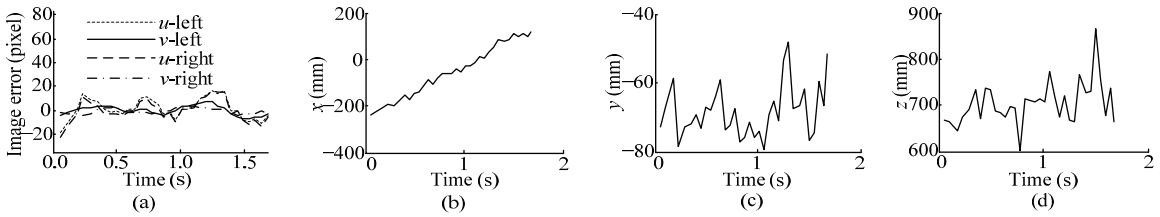

Fig. 16 Experiment results in smooth pursuit when the optimal observation position and motion planning are used. (a) Error curves on image; (b) *x*-coordinates; (c) *y*-coordinates; (d) *z*-coordinates.

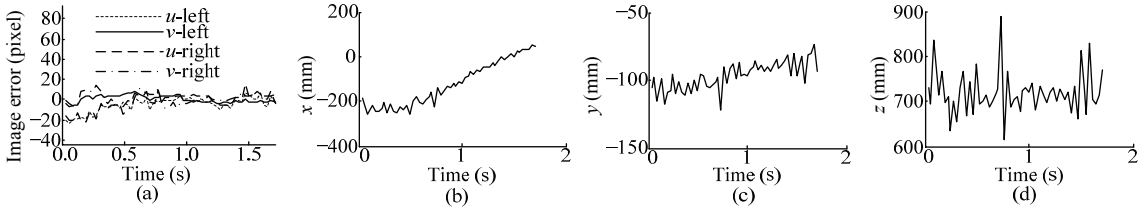

Fig. 17 Contrast experiment results in smooth pursuit when the optimal observation position and motion planning are not used. (a) Error curves on image; (b) *x*-coordinates; (c) *y*-coordinates; (d) *z*-coordinates.

7 Conclusion

In this paper, a new method that imitates smooth pursuit and saccade based on 3D coordinates of target is proposed. The optimal observation position is defined and a method of motion planning for stepper motors is applied in order to control the bionic eye with four stepper motors rapidly and smoothly. The optimal observation position is determined based on the 3D coordinates of the target calculated in the condition of nearly unchanged binocular baseline. The accuracy of the 3D coordinates acquired at the optimal observation position is improved in saccade experiment. The parameters of the stepper motors' motion are obtained via motion planning. They are determined based on the position deviation, the target's angular velocity and the stepper motor's current angular velocity. Experiments show that the stepper motors can move to the given positions with desired angular velocity in schedule time. This work provides a basis for 3D reconstruction of a bionic eye system when the movements of left eye and right eye are independent. However, with the limitation of experiment condition, there are a lot of problems to be solved in future. Firstly, the trajectory of stepper motor can be designed to be parabola shape in order to reduce the lost steps. Secondly, some other measures can be applied to improve the accuracy of 3D coordinates. Thirdly, 3D reconstruction can be realized when the bionic eye is moving like human eye.

Acknowledgment

This study was supported by the National Natural Science Foundation of China under Grant No. 61573347 and in part by the National High Technology Research and Development Program of China ("863 Program") under Grant No. 2015AA042307 and the special fund of Jiangsu Province for the transformation of scientific and technological achievements under Grant BA2015144.

References

[1] Pateromichelakis N, Mazel A, Hache M A, Koumpogiannis T, Gelin R, Maisonnier B, Berthoz A. Head-eyes system and gaze analysis of the humanoid robot Romeo. *Proceedings of IEEE/RSJ International Conference on Intelligent Robots and Systems*, Chicago, USA, 2014, 1374–1379.

[2] Lütkebohle I, Hegel F, Schulz S, Hackel M, Wrede B, Wachsmuth S, Sagerer G. The Bielefeld anthropomorphic robot head 'Flobi'. *Proceedings of IEEE International Conference on Robotics and Automation*, Taipei, Taiwan, 2010, 3384–3391.

[3] Kishi T, Otani T, Endo N, Kryczka P, Hashimoto K, Nakata K, Takanishi A. Development of expressive robotic head for bipedal humanoid robot. *Proceedings of IEEE/RSJ International Conference on Intelligent Robots and Systems*, Osaka, Japan, 2012, 4584–4589.

[4] Zhang L, Sturm J, Cremers D, Lee D. Real-time human motion tracking using multiple depth cameras. *Proceedings of IEEE/RSJ International Conference on Intelligent Robots and Systems*, Chicago, USA, 2014, 2389–2395.

[5] Schwarz L A, Mkhitaryan A, Mateus D, Navab N. Human skeleton tracking from depth data using geodesic distances and optical flow. *Image and Vision Computing*, 2012, **30**, 217–226.

[6] Young L R, Stark L. Variable feedback experiments testing a sampled data model for eye tracking movements. *IEEE Transactions on Human Factors in Electronics*, 1963, **4**, 38–51.

[7] Robinson D A. Models of the saccadic eye movement control system. *Kybernetik*, 1973, **14**, 71–83.

[8] Quaia C, Lefèvre P, Optican L M. Model of the control of saccades by superior colliculus and cerebellum. *Journal of Neurophysiology*, 1999, **82**, 999–1018.

[9] Chen-Harris H, Joiner W M, Ethier V, Zee D S, Shadmehr R. Adaptive control of saccades via internal feedback. *Journal of Neuroscience*, 2008, **28**, 2804–2813.

[10] Chao F, Lee M H, Lee J J. A developmental algorithm for ocular–motor coordination. *Robotics and Autonomous Systems*, 2010, **58**, 239–248.

[11] Robinson D A, Gordon J L, Gordon S E. A model of the smooth pursuit eye movement system, *Biological Cybernetics*, 1986, **55**, 43–57.

[12] Brown C. Gaze controls with interactions and delays. *IEEE Transactions on Systems, Man, and Cybernetics*, 1990, **20**, 518–527.

[13] Deno D C, Keller E L, Crandall W F. Dynamical neural network organization of the visual pursuit system. *IEEE Transactions on Biomedical Engineering*, 1989, **36**, 85–92.

[14] Lunghi F, Lazzari S, Magenes G. Neural adaptive predictor for visual tracking system. *Proceedings of the* 20*th Annual International Conference of the IEEE Engineering in Medicine and Biology Society*, Hong Kong, China, 1998, **20**, 1389–1392.

[15] Avni O, Borrelli F, Katzir G, Rivlin E, Rotstein H. Scanning and tracking with independent cameras-a biologically motivated approach based on model predictive control. *Autonomous Robots*, 2008, **24**, 285–302.

[16] Zhang M, Ma X, Qin B, Wang G, Guo Y, Xu Z, Wang Y, Li Y. Information fusion control with time delay for smooth pursuit eye movement. *Physiological Reports*, 2016, **4**, 1–10.

[17] Santini F, Rucci M. Active estimation of distance in a robotic system that replicates human eye movement. *Robotics and Autonomous Systems*, 2007, **55**, 107–121.

[18] Chinellato E, Antonelli M, Grzyb B J, Del Pobil A P. Implicit sensorimotor mapping of the peripersonal space by gazing and reaching. *IEEE Transactions on Autonomous Mental Development*, 2011, **3**, 43–53.

[19] Song Y, Zhang X. An active binocular integrated system for intelligent robot vision. *Proceedings of IEEE International Conference on Intelligence and Security Informatics*, Washington, USA, 2012, 48–53.

[20] Wang X, Van De Weem J, Jonker P. An advanced active vision system imitating human eye movements. *Proceedings of the* 16*th International Conference on Advanced Robotics*, Montevideo, Uruguay, 2013, 5–10.

[21] Antonelli M, Duran A J, Chinellato E, Pobil A P. Adaptive saccade controller inspired by the primates' cerebellum. *Proceedings of IEEE International Conference on Robotics and Automation*, Washington, USA, 2015, 5048–5053.

[22] Wang Y, Zhang G, Lang H, Zuo B, De Silva C W. A modified image-based visual servo controller with hybrid camera configuration for robust robotic grasping. *Robotics and Autonomous Systems*, 2014, **62**, 1398–1407.

[23] Zhang Z. A flexible new technique for camera calibration. *IEEE Transactions on Pattern Analysis and Machine Intelligence*, 2000, **22**, 1330–1334.

[24] Brown D C. Close-range camera calibration. *Photogrammetric Engineering*, 1971, **37**, 855–866.

[25] Wang Q, Zou W, Zhang F, Xu D. Binocular initial location and extrinsic parameters real-time calculation for bionic eye system. *Proceedings of the* 11*th World Congress on Intelligent Control and Automation*, Shenyang, China, 2014, 74–80.